Bioconjugate Chemistry

Article

pubs.acs.org/bc

Gold Nanoparticles Stabilized with MPEG-Grafted Poly(L-lysine): in Vitro and in Vivo Evaluation of a Potential Theranostic Agent

Alexei A. Bogdanov, Jr.,*[,†,‡] Suresh Gupta,[†] Nadezhda Koshkina,[§] Stuart J. Corr,[§,∥,⊥] Surong Zhang,[†] Steven A. Curley,[§,⊥,#] and Gang Han[¶]

[†]Departments of Radiology and [‡]Cell Biology, University of Massachusetts Medical School, Worcester, Massachusetts 01655, United States

[§]Department of Surgical Oncology, University of Texas M. D. Anderson Cancer Center, Houston, Texas 77030, United States

[∥]Department of Chemistry and the Richard E. Smalley Institute for Nanoscale Science and Technology and [#]Department of Mechanical Engineering and Materials Science, Rice University, Houston, Texas 77251, United States

[⊥]Department of Surgical Research, Baylor College of Medicine, One Baylor Plaza, Houston, Texas 77030, United States

[¶]Department of Biochemistry and Molecular Pharmacology University of Massachusetts Medical School, Worcester, Massachusetts 01655, United States

Supporting Information

ABSTRACT: As the number of diagnostic and therapeutic applications utilizing gold nanoparticles (AuNPs) increases, so does the need for AuNPs that are stable in vivo, biocompatible, and suitable for bioconjugation. We investigated a strategy for AuNP stabilization that uses methoxypolyethylene glycol-*graft*-poly(L-lysine) copolymer (MPEG-gPLL) bearing free amino groups as a stabilizing molecule. MPEG-gPLL injected into water solutions of $HAuCl_4$ with or without trisodium citrate resulted in spherical (Z_{av} = 36 nm), monodisperse (PDI = 0.27), weakly positively charged nanoparticles (AuNP3) with electron-dense cores (diameter: 10.4 ± 2.5 nm) and surface amino groups that were amenable to covalent modification. The AuNP3 were stable against aggregation in the presence of phosphate and serum proteins and remained dispersed after their uptake into endosomes. MPEG-gPLL-stabilized AuNP3 exhibited high uptake and very low toxicity in human endothelial cells, but showed a high dose-dependent toxicity in epithelioid cancer cells. Highly stable radioactive labeling of AuNP3 with ^{99m}Tc allowed imaging of AuNP3 biodistribution and revealed dose-dependent long circulation in the blood. The minor fraction of AuGNP3 was found in major organs and at sites of experimentally induced inflammation. Gold analysis showed evidence of a partial degradation of the MPEG-gPLL layer in AuNP3 particles accumulated in major organs. Radiofrequency-mediated heating of AuNP3 solutions showed that AuNP3 exhibited heating behavior consistent with 10 nm core nanoparticles. We conclude that PEG-pPLL coating of AuNPs confers "stealth" properties that enable these particles to exist in vivo in a nonaggregating, biocompatible state making them suitable for potential use in biomedical applications such as noninvasive radiofrequency cancer therapy.

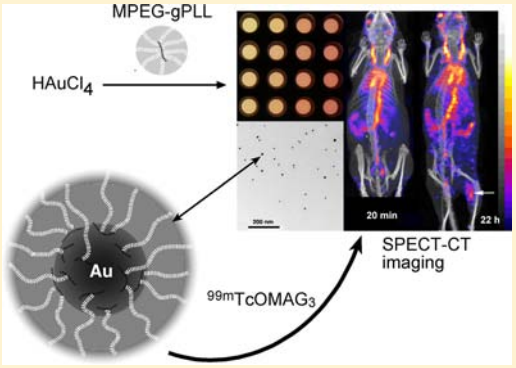

INTRODUCTION

The continuous effort toward AuNP surface modification has demonstrated that the addition of a protective layer to the surface of nanoparticles drastically improves their stability in vivo, while maintaining a small particle size. The protection is usually accomplished by adsorbing and/or chemically orienting polymers,[1−3] thereby generating a layer that becomes sterically and chemically protective due to a lowering of the effective surface energy of the colloidal gold surface. Consequently, surface protection of AuNPs prevents particle aggregation in biological fluids.[4,5]

There are numerous strategies that utilize a combination of reducing/gold colloid capping polymers[6] for the formulation of surface-coated AuNPs. Short di- to tetra-ethylene oxide long PEG-thiols were first suggested for stabilizing AuNPs[1,6] analogous to alkanethiols that are commonly used in stabilizing gold nanocrystals during the synthesis of AuNPs in organic solvent/water systems.[7] Short, low molecular weight PEGs do not bind or activate complement (unless a terminal hydroxyl is exposed on PEG chains[8,9]). However, longer PEG-based mono-[10] or dithiols[11] were shown to be more convenient for AuNP stabilization and functionalization of citrate-reduced AuNPs and enabled in vivo testing of PEG-coated AuNPs.[10,12] These results taken together suggest that an ideal compound for surface coating of AuNPs would have denser PEG-based polymers that were devoid of complement activating activity.

Received: June 10, 2014
Published: December 1, 2014

   dx.doi.org/10.1021/bc5005087 | *Bioconjugate Chem.* 2015, 26, 39−50

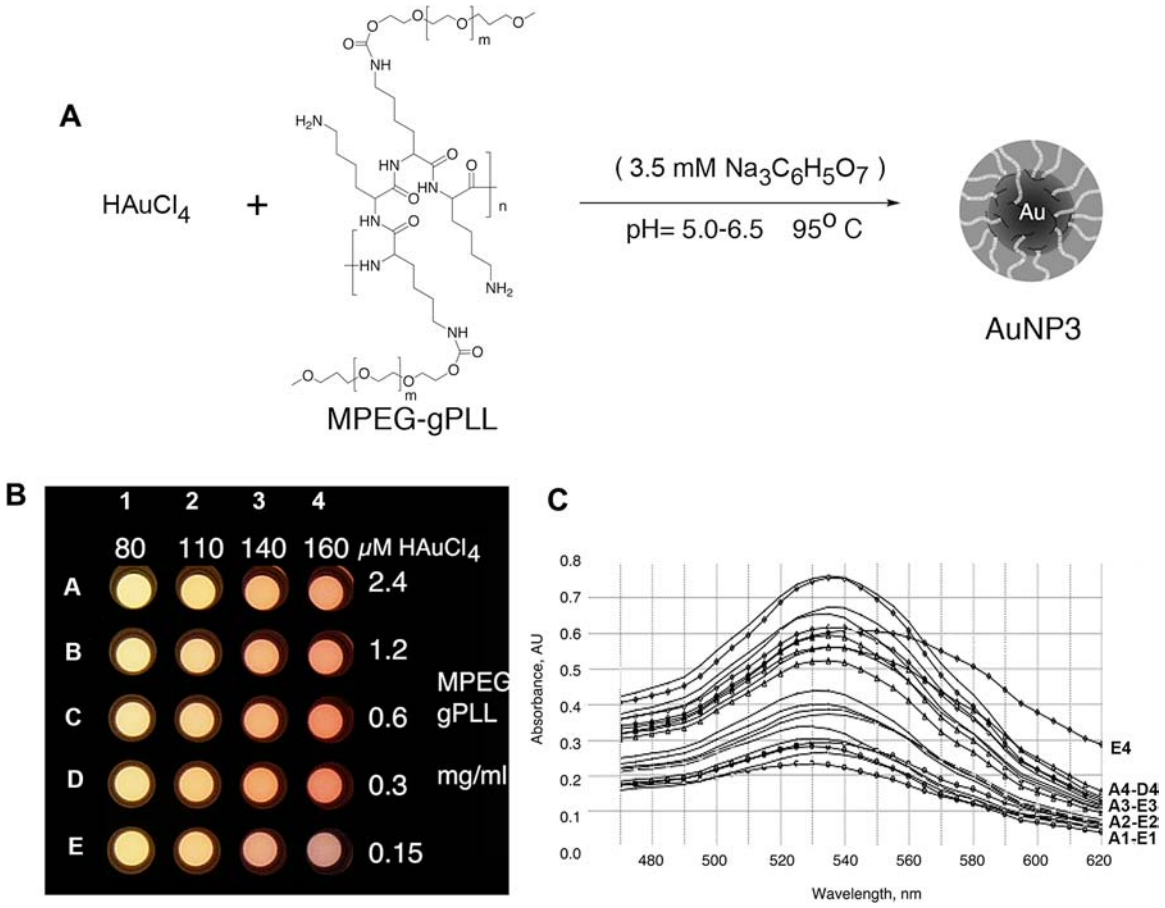

Figure 1. Synthesis and optical properties of MPEG-gPLL-stabilized gold nanoparticles (AuNPs). (A) Schema of water phase synthesis of AuNPs using capping/stabilizing MPEG-gPLL graft copolymer and optional trisodium citrate, n = 110, m=164. (B) Image of the PCR well-plate acquired after the synthesis of AuNPs in the presence of various concentrations of $HAuCl_4$ and MPEG-gPLL. (C) Comparative absorbance spectra showing the positions and intensities of the GNP plasmon peaks measured in the wells of the plate shown in (B) with the corresponding well series indicated on the right.

Such surface-stabilized AuNPs are being increasingly recognized as ideally suited for a number of diagnostic and therapeutic (theranostic) biomedical applications.[13,14] For example, tumors that accumulate AuNPs can be ablated when the AuNPs are heated by radiofrequency (RF) electric fields[15,16] or near-infrared photons[17] so as to produce hyperthermic cytotoxicity in surrounding cells. In addition, the absorption of 100−200 kV photons by AuNPs results in a potentiation of ionizing radiation, suggesting that AuNPs may be useful as radiotherapy enhancing agents in cancer treatment.[18,19] In contrast, nonstabilized AuNPs were shown to be non-bioinert,[20] with mild-to-severe nephrotoxicity being described in several animal species.[21] Thus, the development of biologically safe and effective coating and delivery strategies for AuNPs will be key in bringing this theranostic compound into widespread clinical use.

One existing challenge stemming from the exposed gold and its associated high surface binding energy to biological milieu is the adsorption of proteins that affects nanoparticle−cell interactions.[22] To date almost 120 human plasma proteins have been shown to bind with AuNPs.[23] Protein adsorption prevents rapid aggregation but does not preclude high uptake in the reticuloendothelial system with a concomitant intra-endosomal aggregation in the cells. Consequently, the resultant toxicity of AuNPs[5,24] in vivo is dramatically increased. Moreover, noninvasive RF cancer therapy is less effective at inducing targeted hyperthermia when the AuNPs are aggregated,[25,26] which could limit the usefulness of AuNPs for RF-ablative therapies. Similar to well-known strong thiol−gold interactions, charge-neutral amine/gold surface interactions (which are comparable to weak covalent bonds between gold atoms and the nitrogens of amines[27]) are capable of supporting stabilizing layers on gold nanoparticles. We hypothesized that methoxy(polyethylene glycol)-polylysine conjugates, i.e., MPEG-gPLL graft copolymers that were previously extensively used for delivery of imaging probes (reviewed in ref 28), have a potential use in AuNP stabilization. This potential stems from the relative strength of amine−gold interactions combined with a level of cooperativity of gold interactions with multiple amino groups carried by a single MPEG-gPLL molecule. Therefore, in our work we set forth to (1) investigate the ability of MPEG-gPLL to stabilize and simultaneously to functionalize AuNPs by providing a plurality of amino groups available for further facile conjugation of various ligands to the surface of nanoparticles, and (2) test the heating and electrical properties of the obtained nonaggregating AuNPs for future applications in minimally invasive cancer therapy.

RESULTS

Synthesis and Characterization of MPEG-gPLL and AuNPs. By using alternative conjugation chemistries for

dx.doi.org/10.1021/bc5005087 | Bioconjugate Chem. 2015, 26, 39−50

grafting MPEG5 chains to a PLL backbone (Supporting Information Figure 1S) we obtained graft-copolymers with MPEG chains linked via either very stable urethane bonds (MPEG-gPLL1) or less stable amide bonds with an additional labile ester bond in the MPEG chain (MPEG-gPLL2). Both MPEG-gPLL1 and MPEG-gPLL2 had excellent solubility in water in the pH range of 3−9 and were eluted on Superdex 200 as single peaks (Supporting Information Figure 2S, A). The analysis of the structure of the obtained copolymers showed the presence of all the anticipated structural blocks (Supporting Information Figure 2S, B and C). The PEGylation degree was determined by integrating the total area of ε-CH2 proton peaks corresponding to free and acylated lysine side-chains and calculating the fraction of acylated side chains. For example, Supporting Information Figure 2S shows MPEG-gPLL with a PEGylation degree of 30%. The synthesized MPEG-gPLL1 and 2 contained approximately 25% MPEGylated N-ε-amino groups. Higher numbers of conjugated MPEG5 chains, i.e., more than 30% of the available N-ε-amino groups of PLL,[28] resulted in graft-copolymers that did not support the stabilization of AuNPs.

To synthesize MPEG-gPLL-stabilized AuNP we tested several protocols that included (1) the coaddition of MPEG-gPLL and 3.5 mM trisodium citrate to the solution of $HAuCl_4$ at 95 °C (Figure 1A); (2) the addition of MPEG-gPLL in the absence of citrate at 95 °C; or (3) stabilizing AuNPs by adding MPEG-gPLL at 95 °C to freshly prepared citrate-stabilized AuNPs.[29] All tested protocols resulted in AuNPs with very similar properties regardless of whether MPEG-gPLL1 or MPEG-gPLL2 was used for nanoparticle stabilization. However, the yields of nanoparticle synthesis were 1.5-fold higher in the presence of trisodium citrate. In the absence of citrate the AuNPs formed much more rapidly: it took 2 min in the absence vs 30 min in the presence of 3.5 mM trisodium citrate to obtain nanoparticles with a characteristic absorbance peak at 525 nm in a volume of 10 mL. The presence of free amino groups in MPEG-gPLL was essential for obtaining stable and spherical nanoparticles (Table 1). Succinylated or acetylated MPEG-gPLL1 (i.e., with all free amino groups of MPEG-gPLL1 covalently blocked) did not support the formation of spherical AuNPs and resulted mainly in the formation of 2:1 aspect nanorods (Table 1) with plasmon peak widening and shifting to 575 nm. In control experiments, the addition of the excess of amino-terminated MPEG5000 together with citrate during the synthesis of AuNPs did not result in stable nanoparticles. To obtain the amino-containing AuNPs (AuNP4) stabilized with an oriented MPEG layer we used a mixture of MPEG-thiol and amino-PEG-thiol (1:1, by weight) added in the presence of 3.5 mM trisodium citrate during synthesis of AuNP.

We further studied the effect MPEG-gPLL1 graft copolymer and the concentration of $HAuCl_4$ on AuNP formation using a PCR plate format and a Peltier device with rapid heat exchange (Figure 1B). In order to determine conditions that would result in the formation of AuNPs with the optimal dynamic light scattering and highest plasmon peak intensity characteristics (Figure 1B,C), we varied the concentration of $HAuCl_4$ (80 to 160 μM) and of MPEG-gPLL1 (0.3 to 2.4 mg/mL) during synthesis. The results of these titrations showed that the acceptable concentration range for $HAuCl_4$ was 140−160 μM, while the MPEG-gPLL1 concentration had to be kept above 0.3 mg/mL (Figure 1C).

The AuNP synthesis performed in the presence of 0.14 mM $HAuCl_4$, i.e., at the intermediate tested concentrations of

Table 1. Properties of AuNP Used in This Work

sample	description	hydro-dynamic diameter, (by peak intensity), nm mean ± SD (PDI)	gold core size, nm, mean ± SD,	aggre-gation in PBS, pH 7.4	retention on Bio-Gel P30 mean diameter ± SD	zeta-potential (mV), mean ± SD	amino groups
AuNP	Na_3citrate-capped	13.6 ± 11.0 (0.22)	13.0 ± 4.8	yes	Yes 0.68 ± 0.14	−21.0 ± 10.0	ND
AuNP2 (nanorods 2:1)	Na_3citrate followed by succinylated MPEG5-gPLL1	64.9 ± 20.7 (0.34)	NA	no	Yes	−4.4 ± 7.8	ND
AuNP3	Na_3citrate followed by MPEG5-gPLL1 or MPEG-gPLL2	36.9 ± 12.8 (0.27)	10.4 ± 2.5	no	No 49.6 ± 17.6	+3.7 ± 9.8	1 μmol/AU*
AuNP4	Na_3citrate followed by SH-PEG5-NH2 and MPEG5-SH	98.6 ± 28.1 (0.22)	NA	yes	Yes 34.9 ± 9.8	−2.2 ± 5.8	0.2 mmol/AU*
RbMP-AuNP3	AuNP3 with covalently linked riboflavin monophosphate	55.1 ± 16.2 (0.30)	9.3 ± 2.6	no	No 44.8 ± 10.7	−12.9 ± 7.0	ND

*Moles per absorbance at 530 nm (arbitrary units), ND - not detectable.

dx.doi.org/10.1021/bc5005087 | Bioconjugate Chem. 2015, 26, 39−50

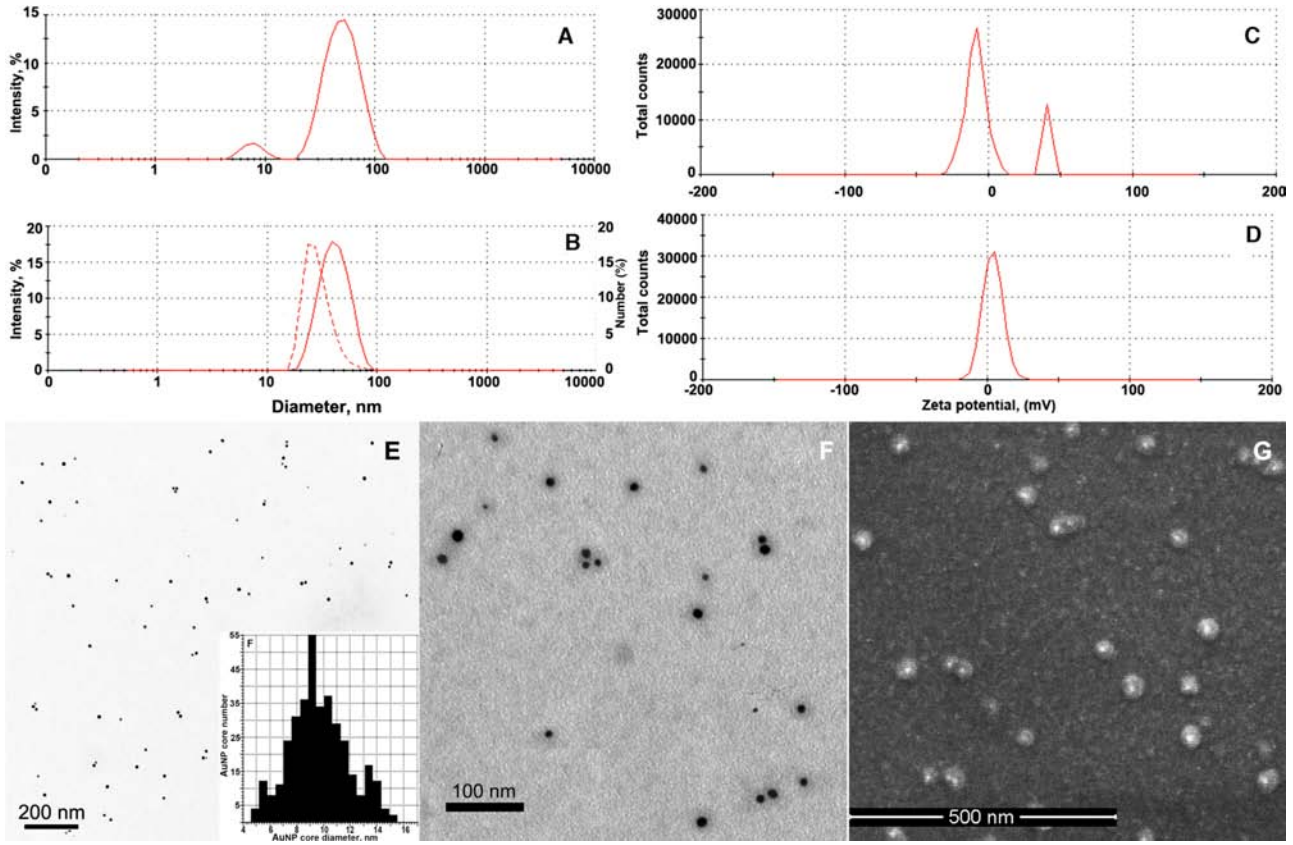

Figure 2. Properties of AuNP3 stabilized with MPEG-gPLL. (A,B) *Z*-average hydrodynamic diameter (LALLS intensity, solid lines) and number size distribution of purified AuNP3 (panel B, hatched line). (C,D) Zeta potential (charge) of AuNPs before (A,C) and after (B,D) the purification. (E) Representative field of view showing the results of transmission electron microscopy of AuNP3s; inset - AuNP3 diameter distribution calculations using image segmentation analysis of large number (n = 360) of AuNP3 gold cores. (F) Uranyl acetate-enhanced contrast staining of the sample shown in panel E. (G) Backscatter (compositional) scanning electron microscopy image of the glass-adsorbed AuNP3.

$HAuCl_4$ and MPEG-gPLL (0.9 mg/mL), resulted in nanoparticles with gold cores of 10.4 ± 2.5 nm diameter as determined by transmission electron microscopy (TEM, Table 1 and Figure 2E) and an average effective hydrodynamic diameter of 36.9 nm due to the presence of the coating layer on their surface ("AuNP3", Table 1). Compared to highly negatively charged citrate-capped AuNPs, AuNP3s were weakly positively charged and carried reactive amino groups (Table 1). The combined evidence of laser light scattering and zeta-potential measurements pointed to the presence of small (6−7 nm) and strongly positively charged molecules of MPEG-gPLL1 that were initially present in AuNP3 reaction mixtures after the synthesis (Figure 2A,C). MPEG-gPLL1 peaks were undetectable in AuNP3 samples following purification by gradient ultracentrifugation and/or ultrafiltration (Figure 2B,D). Ultracentrifugation performed in a step-gradient of nonionic iodixanol allowed separation of MPEG-gPLL-stabilized AuNPs from the bulk of nonbound MPEG-gPLL and enabled the quality of purification to be controlled by analyzing the individual fractions for the presence of amino groups and intensity of AuNP plasmon peak (Supporting Information Figure 4S). Purified MPEG-gPLL1-stabilized AuNP3s did not aggregate in the presence of phosphate anions (PBS, Table 1), nor did they show adsorption on the surface of polysaccharide microporous (i.e., BioGel P-30) and macroporous gel-filtration beads. This allowed the use of size-exclusion chromatography for purity analysis and for purification of AuNP3s from low molecular weight impurities after covalent modification.

The structure and composition of the MPEG-gPLL1 coating surrounding the synthesized AuNP3s was studied in more detail using electron microscopy and gravimetric analysis. TEM of samples following uranyl acetate negative staining revealed the presence of a 9-nm-thick polymer layer on the surface of the AuNP3s that was contrasted with uranyl acetate (Figure 2F). The estimated total diameter of dehydrated AuNP3s (i.e., the core surrounded by the stabilizing layer) was 30.0 ± 4.6 nm. On scanning electron microscopy (SEM) images (Figure 2G), the layer of MPEG-gPLL1 on the surface of nanoparticles was clearly visible and took the appearance of a halo around the gold cores which could easily be identified within the coating layer in the backscattering SEM mode. According to thermogravimetry results, purified and lyophilized AuNP3s contained 34% gold by weight with the rest of the weight balance consisting of hydrated MPEG-gPLL1.

The feasibility of conjugating amine-reactive compounds to the free amino groups of MPEG-gPLL1 attached to AuNPs was tested by linking riboflavin monophosphate (a small negatively charged ligand) using water-soluble carbodiimide. A facile covalent conjugation of phosphate groups to the surface of AuNP3s resulted in phosphamides and a resultant shift of AuNP3 zeta potential from weakly positive to negative (i.e., from average +3.7 to −12.9, Table 1).

Stability and Behavior of MPEG-gPLL-Stabilized AuNPs in Biological Systems. The presence of a layer of

dx.doi.org/10.1021/bc5005087 | *Bioconjugate Chem.* 2015, 26, 39−50

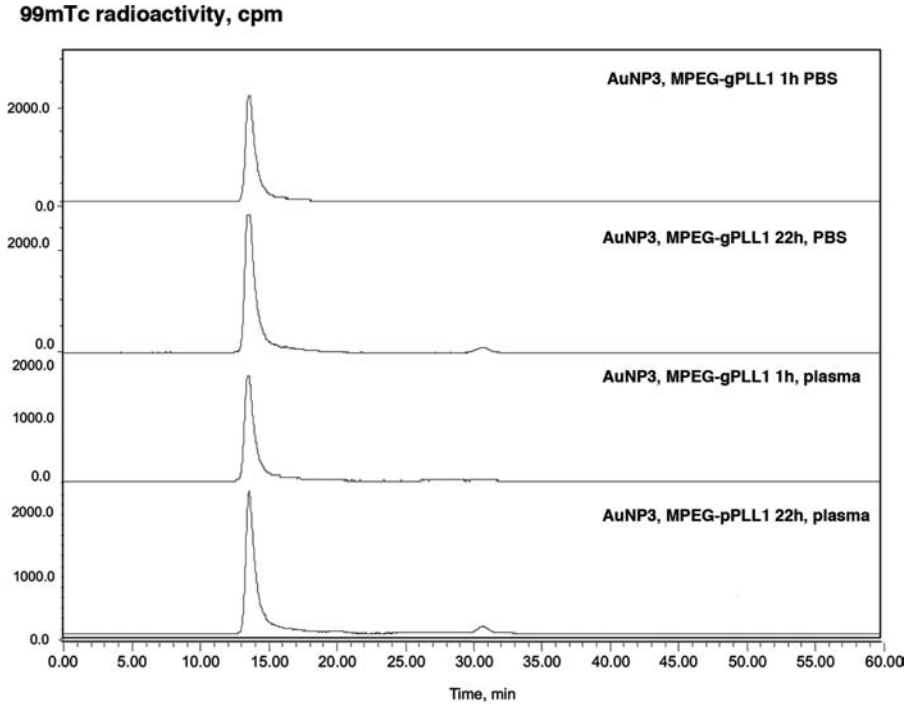

Figure 3. Stability of AuNP3 protective layer. Size-exclusion HPLC profiles of ^{99m}Tc-AuNP3 stabilized with MPEG-gPLL1 that were incubated for 1 and 22 h either in PBS or 75% mouse plasma. HPLC was performed on Superose 6 10/300 GL HPLC size-exclusion column eluted with 20% acetonitrile in 0.1 M TrisHCl, pH 8.0 (0.6 mL/min).

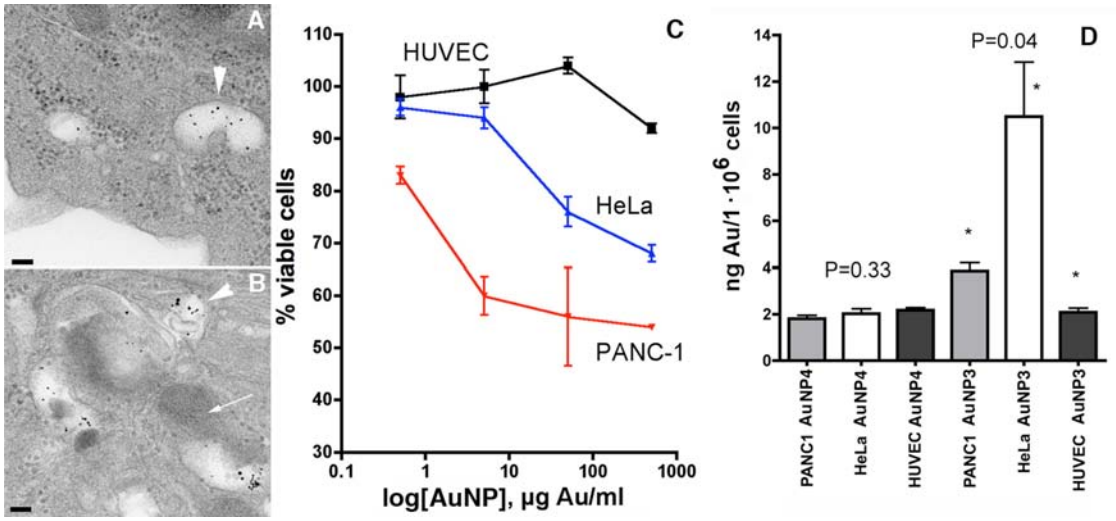

Figure 4. Cell uptake of AuNP3s and cytotoxicity. (A) TEM results showing the presence of individual nonaggregated AuNP3s in the endosomes (arrowhead). (B) Fusion of endosomes (arrowhead) with the lysosome (arrow) coinciding with microaggregation of AuNPs. (C) Gold concentration-dependent cytotoxicity measured in cell culture of normal human endothelial cells (black), HeLa cells (blue), and PANC-1 cells (red). (D) Uptake of AuNP3 and control MPEG-thiol stabilized AuNP4 in HeLa, PANC-1, and normal human endothelial cells expressed as the amount of gold taken up per million cells in culture within 24 h. The uptake of AuNP3s was significantly different between all three cell lines.

MPEG-gPLL1 or MPEG-gPLL2 graft copolymers bearing reactive amino groups suggested that MPEG-gPLL stabilized AuNP could potentially be covalently modified with activated esters of chelates and then labeled with radioactive isotopes for investigating the biodistribution of nanopartciles and tracking the stability of their coating in vitro and in vivo. Initially, we studied the stability of both MPEG-gPLL1- or MPEG-gPLL2-stabilized AuNPs. The particles were covalently modified with S-AcMAG3-NHS, i.e., with S-acetylmercaptoacetyltriglycine residues (S-AcMAG3[30]) that enabled stable labeling of AuNPs with ^{99m}Tc using [^{99m}Tc]-pertechnetate reduction (Figure 3, Supporting Information Figure 5S). The AuNP showed stability of labeling with ^{99m}Tc even after 22 h incubation in PBS and the total loss of radiolabel did not exceed 4% in both cases. The released ^{99m}Tc (as pertechnetate) appeared as minor peaks eluted in the total volume of the column (Figure 3 and Supporting Information Figure 5S). The incubation in the presence of blood plasma at 37 °C resulted in a much greater degree of fragmentation of the MPEG-gPLL2 coating of AuNPs (Supporting Information Figure 5S) than AuNPs stabilized with MPEG-gPLL1: the latter showed no more than 8% loss of ^{99m}Tc in the presence of plasma (Figure

dx.doi.org/10.1021/bc5005087 | Bioconjugate Chem. 2015, 26, 39−50

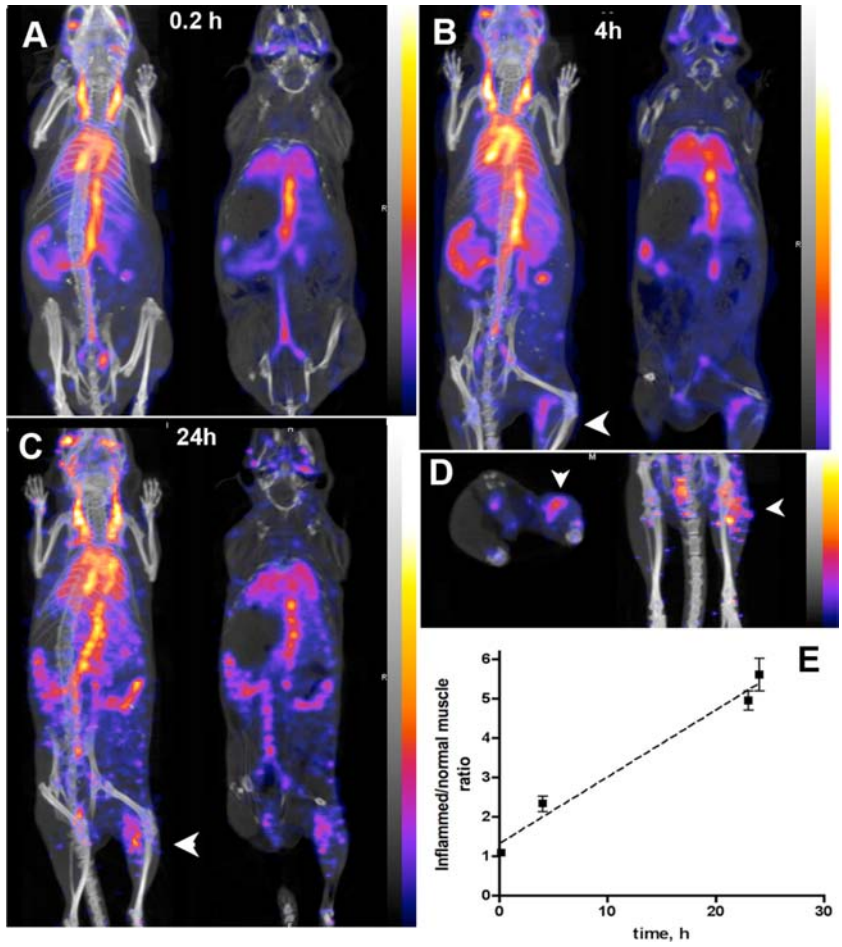

Figure 5. In vivo imaging showing biodistribution and biokinetics of ^{99m}Tc-AuNP3. (A–C) SPECT/CT imaging of ^{99m}Tc-AuNP3 in mouse model of local sterile inflammation in the right extremity at 0.2 (A), 4 (B), and 24 h (C). Coronal maximum intensity pixel projection (MIP) SPECT images fused with CT images at a 600 μCi of ^{99m}Tc-AuNP3 are shown in the left column and representative coronal slice images showing the accumulation of AuNP3 in femoral muscle are shown in the right column. Accumulation in the affected muscle is denoted by arrowheads. The pseudocolor scale representing dose distribution in image voxels is shown on the right. (D) Transverse projection image slice (left) and MIP image (right) of the LPS injected and control contralateral femoral muscle. The accumulation of AuNP3s in the area of inflammation is denoted by arrowheads. (E) Time-dependent increase of the ratio between signals measured in the inflamed and normal contralateral muscle over time.

3). The stability testing of graft copolymers alone (i.e., ^{99m}Tc-labeled and purified MPEG-gPLL1 and MPEG-gPLL2) in PBS and in the presence of plasma revealed fragmentation of the polymers in the presence of plasma and a lack of fragmentation in PBS at 22 h (Supporting Information Figure 3S). However, there was less fragmentation observed in the presence of plasma in the case of MPEG-gPLL1, which dictated selecting MPEG-gPLL1 as the preferred graft copolymer for nanoparticle stabilization in further experiments.

To investigate whether MPEG-gPLL1-stabilized AuNP3s were taken up by normal and cancer human cells in vitro, the nanoparticles were membrane-sterilized and incubated with cells in complete medium (i.e., in the presence of 10% serum) at various concentrations. The measurements of cellular uptake in two cancer cell lines (HeLa, PANC-1) and normal human umbilical vein endothelial cells (HUVEC) showed that cancer cells internalized AuNPs at the following descending order of the uptake of the added amount of AuNPs (concentration range 10–100 μg Au/mL) to different extents with the highest to lowest being HeLa (0.74 ± 0.21%) > PANC-1 (0.70 ± 0.31%) > HUVEC (0.19 ± 0.04%). The uptake in HUVECs was significantly ($p < 0.05$) lower than in epithelioid cancer cell lines. TEM investigation of the uptake revealed the presence of AuNPs in endosomes of cancer cells with most of the nanoparticles exhibiting no binding to the luminal surface of endosomes (Figure 4A). Conversely, in organelles that underwent fusion with lysosomes, nanoparticles appeared more aggregated and associated with the membranes (Figure 4B). PANC-1 cancer cells that showed the highest average level of AuNP3 uptake also exhibited dose-dependent toxicity (50% cell survival at 500 μg Au/mL) whereas normal human endothelial cells exhibited only an 8 ± 2% decrease of cell viability at the same dose (Figure 4C). The low toxicity of AuNP3s for normal endothelium correlated with low uptake of AuNP3s and MPEG-stabilized AuNP 4s (Figure 4D). The uptake of AuNP3s in HeLa cells and PANC-1 was significantly higher and different for all three cell lines ($P = 0.045$), whereas AuNP4 were taken up at the same levels in epithelial cancer cells and HUVEC ($P = 0.33$).

The covalent modification of the MPEG-gPLL1 layer by conjugating S-AcMAG3 residues to the surface of AuNP3s enabled subsequent [^{99m}Tc] labeling of nanoparticles with high yields; the labeling efficiency was in the range of 75–90% of initially added radioactivity. We used [^{99m}Tc]-AuNP3 for in vivo studies that included longitudinal in vivo SPECT imaging and biodistribution experiments. The imaging was performed in

dx.doi.org/10.1021/bc5005087 | Bioconjugate Chem. 2015, 26, 39–50

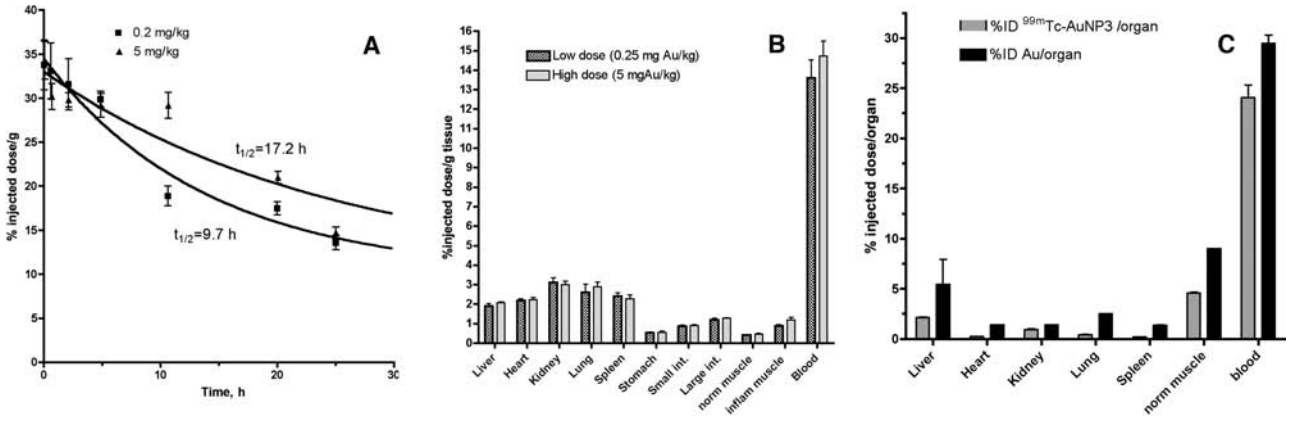

Figure 6. Kinetics of AuNP3 elimination from blood and biodistribution. (A) Blood half-lives determined from a monoexponential fit of ^{99m}Tc-AuNP radioactivity elimination injected at two doses: low − 0.2 mg Au/kg (n = 5/goup); high − 5 mg Au/kg (n = 5/group), r^2 = 0.72−75. (B) Biodistribution in major mouse tissues expressed as fractional dose per gram of tissue weight (n = 5) at low (hatched bars) and high (gray bars) dose of AuNP3 injected I.V. (C) Comparison of AuNP3 biodistribution in the high dose (5 mg Au/kg) animals (n = 4) shown as % injected dose/organ using ^{99m}Tc radioactivity (gray bars) and ICP-MS data (black bars).

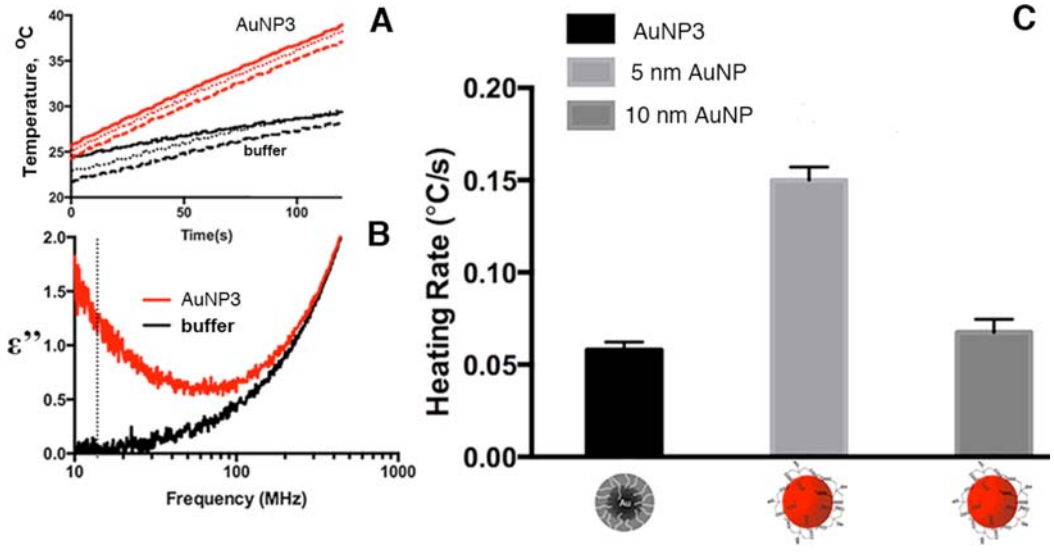

Figure 7. RF heating and electrical properties of AuNP3s compared to citrate-capped AuNPs. Temperature increase (A) and loss tangent (ε'') (B) of AuNP3 solution (0.75 mg gold/mL) versus control (buffer). Dotted line in (B) shows 13.56 MHz RF operating frequency. (C) Differential heating rates of citrate capped AuNPs (average core diameters 5 and 10 nm) compared to AuNP3 (average core diameter 10.4 nm).

a DBA/2 mouse model of locally induced inflammation and in tumor xenograft-bearing athymic mice. Imaging results were corroborated by biodistribution measurements using both decay-corrected ^{99m}Tc radioactivity counts and inductively coupled plasma mass spectrometry (ICP-MS) to measure gold content. Noninvasive SPECT imaging of ^{99m}Tc-AuNP3 showed that after the IV injection the major fraction of the injected radioactivity was contained within the blood pool of mice for an extended period of time (24−26 h, Figure 5). The SPECT imaging results were corroborated by measuring the radioactivity in the blood pool and other major organs (Figure 6A,B). The half-life of ^{99m}Tc-AuNP3 elimination from blood was concentration-dependent and the elimination rate showed first-order kinetics (Figure 6A). Blood sampling followed by separation of blood cells and plasma showed that 89−94% of ^{99m}Tc radioactivity in the blood was associated with plasma and 6−11% with red blood cells and leucocytes. Size-exclusion chromatography of mouse plasma and urine samples obtained in vivo at 4 h post IV injection of ^{99m}Tc-AuNP (Supporting Information Figure 6S) demonstrated that AuNP3 in plasma retained ^{99m}Tc radioactivity, which was eluted as single peaks identical to the initially injected AuNP3 while low ^{99m}Tc radioactivity present in urine was due to the excretion of the fragments of the radioactively labeled MPEG-gPLL1 layer. Only the urine collected from the animals injected with a high dose of AuNP had a minor fraction eluting close to the void volume (Supporting Information Figure 6S). The ICP-MS data showed that with the exception of blood (where the mass of nanoparticles predicted from ^{99m}Tc radioactivity counts was only 20% lower than determined by ICP-MS) the actual gold content in all other major organs was 2−5 times higher than the organ uptake determined based on counts of radioactivity linked to the gold nanoparticle-stabilizing MPEG-gPLL1 layer (Figure 6C).

In experimental disease models, the amounts of AuNP-associated ^{99m}Tc radioactivity detected in the areas of enhanced vascular permeability, i.e., in the experimental inflammatory lesions, as well as in PANC-1 tumors (Supporting Information

dx.doi.org/10.1021/bc5005087 | Bioconjugate Chem. 2015, 26, 39−50

Table 1S) were higher than in control tissues. The target-to-background ratio (i.e., the ratio of normalized radioactivity measured in inflamed extremity versus control nonaffected muscle) increased over time and ranged from 5.2 to 6.1 in areas of inflammation (Figure 5E). Likewise, PANC-1 tumors also showed a markedly increased accumulation of long-circulating AuNP3s with the target-to-background ratio ranging between 2 and 4.

Evaluation of AuNP3s for RF Ablation Applications. We evaluated the use of AuNP3s as a potential vector for applications in noninvasive RF cancer therapy. Figure 7A depicts the temperature data of both citrate-buffered solution of AuNP3 and the same buffer solution lacking AuNP3. The latter was exposed to the RF field after the AuNP3s were separated via ultrafiltration to separately account for ionic Joule heating of the buffer solution. The electrical permittivity properties of the samples were then examined using a permittivity analyzer across the frequency range 10 MHz to 1 GHz. As can be seen in Figure 7B, there is a difference in loss tangent (ε'') between the AuNP3s and the buffer solution, which suggests that AuNP3s will act as a lossy dielectric, i.e., liberating heat when exposed to a radiofrequency range electromagnetic radiation (as is shown in Figure 7A). The differential heating rates of weakly positively charged AuNP3s were then compared to highly negatively charged citrate-capped AuNPs (having diameters 5 and 10 nm) at a similar concentration of particles (Figure 7C). We observed heating profiles that were similar to those of citrate-capped AuNPs of diameter 10 nm. This result is in agreement with our EM measurements of AuNP3 gold core diameters as being approximately 10 nm (Table 1).

DISCUSSION

The goal of our study was to explore the use of a highly hydrophilic covalent graft copolymer of methoxy poly(ethylene glycol) and polylysine (MPEG-gPLL) as a potential stabilizing macromolecule for improving biocompatibility of AuNPs. "Stabilization", i.e., the consequences of intentional decrease of the uniquely large surface energy of gold nanoparticles, has been explored by numerous research groups in the past.[4,5,31] These past efforts included the use of copolymers containing poly(ethylene glycol)[32,33] as a biocompatible synthetic component with controllable structure and length capable of efficient masking of the nanoparticle surface and enabling further potential functionalization of the protective layer.[34] Similarly, the rationale for the use of MPEG-gPLL lies in its biocompatibility and in its capacity to drastically decrease the immunogenicity of any molecule covalently linked to the amino groups of the PLL backbone.[35] Initially designed for MRI,[35] MPEG-gPLL has to date been used for multiple applications in biomedicine and serves as a highly versatile and nontoxic platform for synthesis of a multitude of macromolecular drugs and drug formulations (reviewed in refs 28,36) as well as a gene delivery carrier.[37] The potential benefits of using MPEG-gPLL instead of thiol-PEG or other poly(ethylene oxide) copolymers in AuNP synthesis include: (1) the plurality of free N-ε-amino groups in MPEG-grafted PLL enable cooperative interactions with the gold surface; (2) the "built-in" MPEG protective elements in MPEG-gPLL obviate the need for subsequent modification; (3) the residual amino groups carried by MPEG-gPLL-protected AuNPs enable conjugation to other molecules; and finally, (4) MPEG-gPLL has proven viable as a platform for diagnostic drug development and has performed successfully in past clinical trials.[38]

We investigated in vitro and in vivo properties of AuNPs that were synthesized in the presence MPEG-gPLL, with or without sodium citrate. We established that, indeed, during water-based synthesis the presence of multiple free amino groups in MPEG-gPLL was essential for the formation and stabilization of small and spherical AuNPs (with 10.4 ± 2.5-nm-diameter cores, termed AuNP3), suggesting a critical role for multiple amino groups in stabilization of finite-sized gold surfaces. This was further evidenced by the fact that, after the covalent blocking of the amino groups or after converting MPEG-gPLL into a polyanion by succinylation, the formation of spherical particles was no longer favorable (Table 1). Previous efforts of gold nanoparticle stabilization in the presence of aliphatic monoamines showed that the stabilizing properties of monoamines could be explained by a charge-neutral amine/gold surface interaction that was comparable to weak covalent bonds between gold atoms and the nitrogens of amines.[27] In the case of MPEG-gPLL, multiple amine−gold interactions add cooperativity of copolymer−gold surface interaction that is clearly responsible for the observed stability of AuNP3s against aggregation in the presence of phosphate anions and blood plasma (Table 1, Figure 3). Electron microscopy data pointed to the presence of a layer of MPEG-gPLL on the surface of AuNP3 cores that had a thickness comparable to the gold core diameter (i.e., approximately 9-nm-thick coat vs 10.4 nm core diameter on average), which was in accordance with the results of thermogravimetric analysis.

The next step of AuNP3 testing involved cell culture experiments that suggested overall lower in vitro uptake of MPEG-gPLL-stabilized nontargeted nanoparticles in normal endothelial vs epithelial cancer cells. The overall levels of uptake in cell culture were proportional to the concentration of gold in the incubation media. It should be noted that AuNP3 (which unlike control PEG-thiol stabilized AuNP4 bear weak positive charge) had higher levels of uptake in PANC1 and HeLa cells (Figure 4D). The latter cells overexpress negatively charged heparan sulfate proteoglycans.[39,40] Therefore, differences in the rate of charge-dependent adsorptive endocytosis between cancer cells and normal endothelium is a plausible explanation for the differential uptake of weakly positively charged AuNP3s in cancer cells. Enhanced water phase endocytosis (pinocytosis) of AuNPs, previously shown to be coupled to *Rac1/Ras* activation in cancer cells[41,42] apparently played a less important role considering that normal human endothelial cells showed low uptake of AuNPs regardless of particle coating layer (Figure 4D) and that the uptake of control AuNP4 in normal endothelial cells and epithelioid cancer cells was almost identical. Importantly, the higher observed uptake of AuNP3 in cancer cells compared to normal endothelial cells was associated with pronounced toxicity (Figure 4C) suggesting a potential theranostic use of these gold nanoparticles.

Further, we tested whether the dense coating of AuNP3 with PEGylated copolymer would promote long circulation and extravasation in animal models of experimental sterile inflammation (myositis) and cancer (PANC-1 xenograft model). In vitro testing of AuNP3s that were stabilized with stable MPEG-gPLL1 copolymer retained integrity in plasma or PBS for at least 22 h (Figure 3), which suggested a potential for long circulation of AuNP3s in vivo. The IV administration of [^{99m}Tc]-labeled AuNP3s in mice resulted in excellent blood pool contrast: even at a low injected dose of gold (0.2 mg/kg) AuNP3 showed a half-life of 9.7 h in circulation while a

dx.doi.org/10.1021/bc5005087 | *Bioconjugate Chem.* 2015, 26, 39−50

continuous time-dependent accumulation in the area of experimental inflammation was clearly evident (Figures 5 and 6). It should be noted that long circulation with a plasma half-life of 14.6 ± 3.3 h (first-order elimination in vivo) has been reported previously in mice after an I.V. injection of 1500 times higher doses of MPEG-thiol stabilized AuNPs for CT imaging (0.6 g gold/kg body weight).[10] Our data suggests that the MPEG-gPLL1 layer is also capable of providing AuNPs with efficient protection against rapid clearance in vivo with the additional benefit of multiple free amino groups available on AuNP3 surface for modification with other adaptor molecules including targeting ligands. However, the use of the MPEG-gPLL1 layer did not prevent the in vivo uptake of a minor fraction of AuNP3 that was retained in the organs of reticuloendothelial system either as a result of incomplete coating, or as a result of constitutive uptake from plasma with subsequent degradation of the stabilizing layer of MPEG-gPLL1 (Figure 6C).

The in vivo results obtained in mouse models are clearly relevant to the proposed use of AuNPs as vectors for noninvasive RF radiation-induced ablation of solid tumors that require lossy dielectric nanoparticles[25] (see Figure 7). The prevention of aggregation of these particles is especially critical, since in addition to size, concentration of gold, and the presence of surface charge the heating rates of AuNPs were shown to be negatively affected by the presence of particle aggregates in target cancer cells.[25] The time selected for RF exposure and the AuNP concentrations were similar to those used in vivo by our group previously[15] in which case it was confirmed that a 10 min RF exposure of mice injected with AuNP conjugates did not cause any serious damage to vital organs. We anticipate that the levels of AuNPs in organs will be low (Figure 6 B,C), and due to the normal function of vasculature in these organs, the heating will be dissipated by intensive circulation. In tumors the blood vasculature is slow and inefficient, and therefore, heat dissipation is ineffective[43] causing a localized tumor-specific RF-induced hyperthermia. Further work is currently underway to assess the RF-induced heating efficacies of AuNP3 in both in vitro and in vivo environments.

CONCLUSIONS

In conclusion, coating of AuNPs with a layer of biocompatible graft copolymer during synthesis in the water phase resulted in nanosized single core nanoparticles exhibiting a highly improved stability in solutions containing physiological anions. The improved stability in biological fluids and, as a consequence, long circulation times in vivo were observed in the case of AuNP3 coated with more stable MPEG-gPLL lacking ester bonds. The ability of AuNP3s to accumulate at the sites of abnormal vascular permeability such as sterile inflammation in vivo while resisting aggregation after cellular uptake makes them useful for inducing either direct or RF heating-induced cytotoxicity in cancer cells and suggest the substantial therapeutic and diagnostic potential of AuNP3s. In the future, the ability to fine-tune the number of chemically reactive amino groups on the surface of AuNP3s as well as AuNP core diameters will allow us to further functionalize these nanoparticles and improve the selectivity of their accumulation in tumors, as well as their RF heating rates, thus making them suitable for treating cancer by using localized RF therapy. At the same time, our research demonstrated that the chemistry of stabilizing graft copolymer can be potentially used as a tool for optimizing the required in vivo stability by making the stabilizing layer on the surface of AuNP either more susceptible or more resistant to biodegradation.

EXPERIMENTAL PROCEDURES

Synthesis of Gold Nanoparticles. *(1). Optimization in PCR Plate Format.* MPEG-gPLL1 (PLL grafted with MPEG-carboxymethyl-NHS ester) was synthesized and purified as described in the Supporting Information. MPEG-gPLL1 (120 mg/mL in 35 mM trisodium citrate) was serially diluted 2× in a 96-well titer plate. $HAuCl_4$ solution was diluted to 160, 140, 110, and 80 μM in H_2O. 0.2 mL of these solutions were placed in polypropylene PCR plates (USA Scientific), sealed, and heated to 95 °C using a PCR Peltier thermocycler (PTC-200, MJ Research, Watertown MA). After 5 min, 20 μL of serially diluted solutions of MPEG-gPLL1 were added to the wells of the PCR plate using a multipipette and the plate was resealed and heated at 95 °C for an additional 30 min.

In order to establish the position of the AuNP plasmon resonance peak, the plate was quickly cooled to 0 °C in the thermocycler unit and the contents of the wells were transferred to 96-well plates to measure the absorbance spectra in the range of 400−700 nm using a Spectramax M5 plate reader (Molecular devices).

(2). General AuNP Scale-Up Synthesis Procedure. A 0.14 mM solution of $HAuCl_4$ was prepared in 100 mL of degassed deionized H_2O saturated with nitrogen, using an internal probe to monitor temperature. The solution was quickly heated to 95 °C for 5 min using a water jacket, and subsequently a solution of MPEG-gPLL1 or MPEG-gPLL2 (26 mg/mL in 0.1 M trisodium citrate) was injected into the solution of $HAuCl_4$ in a volume of 3.5 mL with stirring. In some experiments the synthesis was performed in the absence of trisodium citrate by using a solution of MPEG-gPLL in water (26 mg/mL). The final concentration of residual amino groups in the AuNP reaction mixture was approximately 0.4 mM. The heating continued for 15 min and the AuNP reaction mixture was immersed in an ice/water mixture followed by filtering through a 0.22 μm membrane using sterile Steriflip-GV PVDF membrane units (Millipore) for storage prior to the purification. To obtain control MPEG-coated AuNPs (AuNP4), $HAuCl_4$ solution (0.14 mM, 100 mL) was treated with a mixture of 50 mg/mL mono aminePEG5000-thiol and 50 mg/mL MPEG5000 thiol (JenKem Technology, Allen TX) in 3.5 mL of 0.1 M trisodium citrate that was added to $HAuCl_4$ solutions in place of MPEG-gPLL1 or MPEG-gPLL2.

Purification of AuNPs. The separation from free MPEG-gPLL was accomplished by loading 1 mL of AuNP3s concentrated in Amicon Ultra 4 YM-100 centrifuge membrane concentrators (EMD-Millipore, Billerica MA) on top of a step-gradient consisting of 0.2 mL 50% Opti-Prep (60% Iodixanol solution in saline, Sigma-Aldrich, St. Louis MO) with the initial density 1.32 g/mL, followed by 4 mL of 8% solution of Opti-Prep in 0.03 M Hepes, pH 7.5, and centrifuged in a SW55.1 Ti rotor (Beckman) at 40 000 rpm (RCF 152 000 *g*) for 40 min. The bottom 0.4 mL fraction was collected, vortexed, and washed with 20 mM Hepes, 0.1 M NaCl, pH 8.0 using Amicon Ultra 4 YM-100 centrifuge membrane concentrators as suggested by the manufacturer. After the washings, the particles were pooled and lyophilized. The lyophilized particles were reconstituted in water at 10 mg/mL for further experiments. Before thermogravimetric analysis, extensively dialyzed and lyophilized AuNP3 were dried under high vacuum for 3 days.

dx.doi.org/10.1021/bc5005087 | *Bioconjugate Chem.* 2015, 26, 39−50

The purity of nanoparticles was determined using a Superdex 200 size-exclusion HPLC column (GE-Healthcare Life Sciences) eluted with 0.1 M ammonium acetate buffer, pH 7.0.

Linking of MAG3-NHS Ester to AuNPs and ^{99m}Tc Labeling. The covalent modification of MPEG-gPLL AuNPs with *S*-mercaptoacetyldiglycylglycine NHS ester, (S-AcMAG3-NHS, Kerafast, Boston MA) was performed as described.[44] Nonbound MAG3 was removed using Bio-Spin30 centrifugation minicolumns (Bio-Rad) as described by the manufacturer, or on a Sephadex G25m 10 × 1 cm column (Sigma-Aldrich) using gravity size-exclusion chromatography. The labeling procedure that involved the reduction of ^{99m}Tc(VII) pertechnetate with Sn(II) with simultaneous deprotection of thiols is described elsewhere.[44] The radiolabeling purity was determined using ITLC-G and size exclusion HPLC on a Superose 6 10/300 GL column (GE-Healthcare Life Sciences). The stability of labeling was tested by incubating ^{99m}Tc-labeled AuNP3 in the presence of 75% mouse plasma with subsequent analysis of samples using a Superose 6 10/300 GL column.

Conjugation of Riboflavin-5′-Monophosphate. Conjugation of RbMP was accomplished using phosphamide bond formation as suggested in ref 45. Briefly, 0.07 mmol of RbMP in 0.5 mL of 0.2 M 1-methylimidazole was mixed with 0.14 mmol of EDC in 0.5 mL water on ice for 10 min and the resulting mixture was added to 0.2 mL of AuNP3 (1 mg solid) dissolved in 0.2 M $NaHCO_3$. The RbMP-conjugated nanoparticles were purified by dialysis and the absorbance ratios at 445 and 525 nm (i.e., plasmon peak maximum) were determined for the control and conjugated AuNPs, respectively. The extinction coefficient of RbMP at 445 nm is 13 000 $[mol{\cdot}cm]^{-1}$.

Cell Culture Experiments. These were performed in human umbilical vein endothelial cells (HUVEC), HeLa, and PANC-1 cells. HUVEC cells were grown in 5% FBS and complete endothelial cell growth medium (EGM, Cambrex, Baltimore, MD) until confluent. PANC-1 cells were grown in 10% FCS and DMEM and HeLa cells were grown in 10% EMEM. Cells were incubated for 24 h with various concentrations of AuNP3, [^{99m}Tc]-labeled AuNP3s, or [^{99m}Tc]-labeled AuNP4 after which cell uptake was determined by gamma counting of HBSS-washed cell suspensions and cytotoxicity was determined in attached cells. Cytotoxicity was measured using a 96-well format and a standard WST reagent assay by measuring the formation of red formazan compound at 500 nm using a plate reader. The WST signal was normalized using background (reference) measurements at 650 nm.

High-Resolution Transmission Electron Microscopy. TEM characterization of nanoparticles was performed by incubating AuNPs diluted with 1:10 PBS on Formvar coated grids stabilized with evaporated carbon film with or without negative staining with 1% uranyl acetate and further examination under EM (FEI Tecnai 12 Spirit, at 100−140 K magnification). SEM experiments were performed using a FEI Quanta 200 FEG MKII scanning electron microscope. Nanoparticle core size measurements were performed by segmenting images representing four TEM fields of view with a total of n = 300−400 AuNP cores (IP Lab Spectrum, BD Biosciences). The areas of cores were determined by calibrated segmentation, average diameters were generated for each AuNP core assuming circular symmetry, and the results presented as a histogram. Cell culture samples were prepared as follows: PANC-1 cells were treated with 0.1 mg/mL of AuNP3 in cell culture medium and fixed on the following day for 24 h with 1 M sodium cacodylate buffer (pH 7.4) containing 3% glutaraldehyde and 2% formaldehyde. Samples were then washed with 0.1% tannic acid/1 M sodium cacodylate and treated with 1% osmium tetroxide. Finally, samples were stained with 1% uranyl acetate, dehydrated with ethanol, and embedded in LX-112 medium. After polymerization, samples were cut on a microtome and double stained with uranyl acetate/lead citrate. Imaging was done using a JEM1010 transmission electron microscope (Jeol USA, Inc. Boston, MA).

Animal Experiments. The animal protocol involving ^{99m}Tc-labeled, S-AcMAG3-NHS modified AuNP3 injections was approved by the UMMS IACUC committee. To induce local sterile inflammation, mice (DBA/2Ncr, n = 7/group) were implanted with 0.1 mL of 50% Matrigel (Beckton-Dickinson) containing 5 μg LPS from *E. coli* (Sigma-Aldrich, St. Louis, MO) by injecting the ice-cold Matrigel solution using a 21 gauge needle syringe in the right femoral muscle 16 h before the experiment. The left muscle was implanted with the same volume of Matrigel containing no LPS.

The ectopic tumor model was obtained by implanting 1 × 10^6 PANC-1 cells in the right flank of female nu/nu mice (n = 8). Tumors reached the size of 0.5 cm in diameter in 3 weeks after which animals were injected IV with 0.2 mL of ^{99m}Tc-AuNP3 (600 μCi/animal) at a single dose of 0.2 mg Au/kg. The biodistribution was performed at 22 h post injection.

For SPECT/CT imaging, the animals were anesthetized with 1.8% isoflurane/oxygen, and imaged 10 min, 4 h, 24 h, and 26 h after the injection of ^{99m}Tc-AuNP3 (0.2 mg gold/kg) using NanoSPECT/CT (Bioscan). Acquisition time was approximately 30 min. The CT and SPECT reconstruction was performed using InVivoScope 1.37 software (Bioscan) and images were quantified using a volume-of-interest (VOI) approach. Blood radioactivity over time in live animals was quantified using the InVivoScope image postprocessing tool after defining the VOI. To select cylindrical VOI we first selected a circular region-of-interest from the transverse projection image reconstruction and then selected the length of the cylinder from the maximum intensity projection image. Imaging at 26 h was used to determine inflammation/background ratio and the blood pool radioactivity $F_b = k(VOI_{heart}/VOI_{total\_body}) \times$ injected_dose, where k is the radioactivity decay correction factor and VOI is the sum of signals in the volume of interest.

For a biodistribution study in LPS-induced inflammation model the animals were injected with two different doses of AuNP3:0.2 and 7.5 mg gold/kg (n = 7/group, radioactivity dose 600−650 μCi ^{99m}Tc/animal). Blood sampling was performed at various time points by nicking the tail vein, the blood samples were weighed, and radioactivity in blood was counted and normalized for weight and radioactivity decay. The stability in plasma and urine was determined at 4 h post IV injection by collecting the blood sample (0.1 mL) in heparinized tubes, sedimenting the blood cells at 14 000 g and determining the radioactivity in blood cells and plasma separately. Plasma fractions were analyzed by HPLC on Superose6 GL (1 × 30 cm) HPLC size-exclusion column eluted with 20% acetonitrile in 0.1 M TrisHCl, pH 8.0 (0.6 mL/min). The animals were sacrificed after 22 h post I.V. injection and the biodistribution of ^{99m}Tc-AuNP3 was determined by using gamma-counting.

For ICP-MS (Galbraith Laboratories, Inc.) the major organs of mice and muscle samples were weighed, frozen, and lyophilized. Lyophilized samples were then dissolved in a mix of HNO_3:HCl (1:3 vol/vol).

dx.doi.org/10.1021/bc5005087 | *Bioconjugate Chem.* 2015, 26, 39−50

RF-Heating Experiments. The RF-induced heating characteristics of solutions of AuNP3s at a concentration of 0.750 mg Au/mL were studied using the setup previously described.[25] Samples were placed in a 1.3 mL quartz cuvette held by a custom-designed Teflon holder mounted to an adjustable rotary stage under open air conditions at ambient room temperature as described previously. The cuvette was placed 0.8 cm from the transmission head of the RF-field generator located at an arbitrary point on the $X-Y$ plane (7.6 cm, 10.2 cm) with an 8 cm air gap between transmitting and receiving heads. The solutions were then exposed to the high voltage RF fields (90 kV/m, as discussed below) at 950 W generator power (13.56 MHz operating frequency). Temperatures were recorded every 0.1625 s with an infrared camera (FLIR SC 6000, FLIR Systems, Inc., Boston, MA) for a duration of 120 s or until the sample reached 70 °C (higher temperatures were not attempted to prevent electrical arcing due to excess water evaporation). The temperatures of four control areas were also recorded to subtract any stray heating effects from the instrument and/or Teflon holder.

Permittivity Analysis. Complex permittivity measurements were taken using an Agilent 85070E high-temperature coaxial dielectric probe (Agilent Technologies, Santa Clara, CA) connected to an Agilent E4991A impedance analyzer across the frequency range 10 MHz to 1 GHz. Approximately 800 logarithmic data points were taken across the specified frequency range with each measurement taken 10 times.

■ ASSOCIATED CONTENT

Ⓢ Supporting Information

Experimental details and supporting results. This material is available free of charge via the Internet at http://pubs.acs.org.

■ AUTHOR INFORMATION

Corresponding Author

*Tel: 508-856-5571. E-mail: Alexei.Bogdanov@umassmed.edu.

Notes

The authors declare no competing financial interest.

■ ACKNOWLEDGMENTS

Funding has been provided by NIH grants 2R01EB000858-10, 5R01AG034901-04 (to A.B.), R21EB017980-01 (to S.Z.), R01MH103133, Human Frontier Science Program, UMass CVIP award (to G.H), and 5U54CA143837-05, to S.A.C. The project was supported also by Awards S10RR027897 and S10RR021043 from the National Center For Research Resources. We are grateful to Drs. Guozheng Liu (Department of Radiology) and Miles Smith (The UMMS Small Animal Imaging Core Facility) for their expertise in animal experimentation, to Dr. Mary Mazzanti for editorial expertise, and to Dr. Gregory Hendricks (electron microscopy support).

■ ABBREVIATIONS

MAG3, *S*-mercaptoacetyldiglycylglycyl-; MPEG-pPLL, covalent graft copolymer of methoxy poly(ethylene glycol) and polylysine; AuNP3, gold nanoparticles stabilized with MPEG-gPLL; ICP-MS, inductively coupled plasma mass spectrometry; ^{99m}Tc- AuNP3, ^{99m}Tc-labeled AuNP3 bearing *S*-mercaptoacetyldiglycylglycine residues; MPEG, methoxypoly(ethylene glycol); MIP, maximum intensity pixel projection; RbMP, riboflavin-5′-monophosphate; SPECT, Single-photon emission computed tomography

■ REFERENCES

(1) Zheng, M., Davidson, F., and Huang, X. (2003) Ethylene glycol monolayer protected nanoparticles for eliminating nonspecific binding with biological molecules. *J. Am. Chem. Soc. 125*, 7790−7791.

(2) Sakai, T., and Alexandridis, P. (2005) Mechanism of gold metal ion reduction, nanoparticle growth and size control in aqueous amphiphilic block copolymer solutions at ambient conditions. *J. Phys. Chem. B 109*, 7766−7777.

(3) Liu, Y., Shipton, M. K., Ryan, J., Kaufman, E. D., Franzen, S., and Feldheim, D. L. (2007) Synthesis, stability, and cellular internalization of gold nanoparticles containing mixed peptide-poly(ethylene glycol) monolayers. *Anal. Chem. 79*, 2221−2229.

(4) Walkey, C. D., Olsen, J. B., Guo, H., Emili, A., and Chan, W. C. (2012) Nanoparticle size and surface chemistry determine serum protein adsorption and macrophage uptake. *J. Am. Chem. Soc. 134*, 2139−2147.

(5) Monopoli, M. P., Aberg, C., Salvati, A., and Dawson, K. A. (2012) Biomolecular coronas provide the biological identity of nanosized materials. *Nat. Nanotechnol. 7*, 779−786.

(6) Zheng, M., Li, Z., and Huang, X. (2004) Ethylene glycol monolayer protected nanoparticles: synthesis, characterization, and interactions with biological molecules. *Langmuir 20*, 4226−4235.

(7) Brust, M., Walker, M., Bethell, D., Schiffrin, D., and Whyman, R. (1994) Synthesis of thiol-derivatised gold nanoparticles in a two-phase Liquid−Liquid system. *J. Chem. Soc., Chem. Commun. 7*, 801−802.

(8) Marchand, C., Bachand, J., Perinet, J., Baraghis, E., Lamarre, M., Rivard, G. E., De Crescenzo, G., and Hoemann, C. D. (2010) C3, C5, and factor B bind to chitosan without complement activation. *J. Biomed. Mater. Res., Part A 93*, 1429−1441.

(9) Benesch, J., and Tengvall, P. (2002) Blood protein adsorption onto chitosan. *Biomaterials 23*, 2561−2568.

(10) Cai, Q. Y., Kim, S. H., Choi, K. S., Kim, S. Y., Byun, S. J., Kim, K. W., Park, S. H., Juhng, S. K., and Yoon, K. H. (2007) Colloidal gold nanoparticles as a blood-pool contrast agent for X-ray computed tomography in mice. *Invest. Radiol. 42*, 797−806.

(11) Eck, W., Craig, G., Sigdel, A., Ritter, G., Old, L. J., Tang, L., Brennan, M. F., Allen, P. J., and Mason, M. D. (2008) PEGylated gold nanoparticles conjugated to monoclonal F19 antibodies as targeted labeling agents for human pancreatic carcinoma tissue. *ACS Nano 2*, 2263−2272.

(12) Eck, W., Nicholson, A. I., Zentgraf, H., Semmler, W., and Bartling, S. (2010) Anti-CD4-targeted gold nanoparticles induce specific contrast enhancement of peripheral lymph nodes in X-ray computed tomography of live mice. *Nano Lett. 10*, 2318−2322.

(13) West, J. L., and Halas, N. J. (2003) Engineered nanomaterials for biophotonics applications: improving sensing, imaging, and therapeutics. *Annu. Rev. Biomed. Eng. 5*, 285−292.

(14) Han, G., Ghosh, P., and Rotello, V. M. (2007) Functionalized gold nanoparticles for drug delivery. *Nanomedicine (London) 2*, 113−123.

(15) Glazer, E. S., Zhu, C., Massey, K. L., Thompson, C. S., Kaluarachchi, W. D., Hamir, A. N., and Curley, S. A. (2010) Noninvasive radiofrequency field destruction of pancreatic adenocarcinoma xenografts treated with targeted gold nanoparticles. *Clin. Cancer Res. 16*, 5712−5721.

(16) Glazer, E. S., and Curley, S. A. (2010) Radiofrequency field-induced thermal cytotoxicity in cancer cells treated with fluorescent nanoparticles. *Cancer 116*, 3285−3293.

(17) Krishnan, S., Diagaradjane, P., and Cho, S. H. (2010) Nanoparticle-mediated thermal therapy: evolving strategies for prostate cancer therapy. *Int. J. Hyperthermia 26*, 775−789.

(18) Butterworth, K. T., Coulter, J. A., Jain, S., Forker, J., McMahon, S. J., Schettino, G., Prise, K. M., Currell, F. J., and Hirst, D. G. (2010) Evaluation of cytotoxicity and radiation enhancement using 1.9 nm gold particles: potential application for cancer therapy. *Nanotechnology 21*, 295101.

(19) Hainfeld, J. F., Dilmanian, F. A., Zhong, Z., Slatkin, D. N., Kalef-Ezra, J. A., and Smilowitz, H. M. (2010) Gold nanoparticles enhance

the radiation therapy of a murine squamous cell carcinoma. *Phys. Med. Biol. 55*, 3045−3059.
(20) Brown, C. L., Whitehouse, M. W., Tiekink, E. R., and Bushell, G. R. (2008) Colloidal metallic gold is not bio-inert. *Inflammopharmacology 16*, 133−137.
(21) Simpson, C. A., Huffman, B. J., Gerdon, A. E., and Cliffel, D. E. (2010) Unexpected Toxicity of Monolayer Protected Gold Clusters Eliminated by PEG-Thiol Place Exchange Reactions. *Chem. Res. Toxicol. 23*, 1608−1616.
(22) Walkey, C. D., Olsen, J. B., Song, F., Liu, R., Guo, H., Olsen, D. W., Cohen, Y., Emili, A., and Chan, W. C. (2014) Protein corona fingerprinting predicts the cellular interaction of gold and silver nanoparticles. *ACS Nano 8*, 2439−2455.
(23) Tenzer, S., Docter, D., Rosfa, S., Wlodarski, A., Kuharev, J., Rekik, A., Knauer, S. K., Bantz, C., Nawroth, T., Bier, C., Sirirattanapan, J., Mann, W., Treuel, L., Zellner, R., Maskos, M., Schild, H., and Stauber, R. H. (2011) Nanoparticle size is a critical physicochemical determinant of the human blood plasma corona: a comprehensive quantitative proteomic analysis. *ACS Nano 5*, 7155−7167.
(24) Cedervall, T., Lynch, I., Lindman, S., Berggard, T., Thulin, E., Nilsson, H., Dawson, K. A., and Linse, S. (2007) Understanding the nanoparticle-protein corona using methods to quantify exchange rates and affinities of proteins for nanoparticles. *Proc. Natl. Acad. Sci. U. S. A. 104*, 2050−2055.
(25) Corr, S. J., Raoof, M., Mackeyev, Y., Phounsavath, S., Cheney, M. A., Cisneros, B. T., Shur, M., Gozin, M., McNally, P. J., Wilson, L. J., and Curley, S. A. (2012) Citrate-capped gold nanoparticle electrophoretic heat production in response to a time-varying radiofrequency electric-field. *J. Phys. Chem. C 116*, 24380−24389.
(26) Raoof, M., Corr, S. J., Kaluarachchi, W. D., Massey, K. L., Briggs, K., Zhu, C., Cheney, M. A., Wilson, L. J., and Curley, S. A. (2012) Stability of antibody-conjugated gold nanoparticles in the endolysosomal nanoenvironment: implications for noninvasive radiofrequency-based cancer therapy. *Nanomedicine 8*, 1096−1105.
(27) Leff, D., Brandt, L., and Heath, J. (1996) Synthesis and characterization of hydrophobic, organically-soluble gold nanocrystals functionalized with Primary Amines. *Langmuir 12*, 4723−4730.
(28) Bogdanov, A. J., Mazzanti, M., Castillo, G., and Bolotin, E. (2012) Protected graft copolymer (PGC) in imaging and therapy: a platform for the delivery of covalently and non-covalently bound drugs. *Theranostics 2*, 553−576.
(29) Frens, G. (1973) Controlled nucleation for the regulation of the particle size in monodisperse gold suspensions. *Nat. Phys. Sci. 241*, 20−22.
(30) Vanbilloen, H. P., Bormans, G. M., De Roo, M. J., and Verbruggen, A. M. (1995) Complexes of technetium-99m with tetrapeptides, a new class of 99mTc-labelled agents. *Nucl. Med. Biol. 22*, 325−338.
(31) Dumur, F., Guerlin, G., Dumas, E., Bertin, D., Gigmes, D., and Mayer, C. (2011) Controlled spontaneous generation of gold nanoparticles assisted by dual reducing and capping agents. *Gold Bull. 44*, 119−137.
(32) Murthy, A. K., Stover, R. J., Borwankar, A. U., Nie, G. D., Gourisankar, S., Truskett, T. M., Sokolov, K. V., and Johnston, K. P. (2013) Equilibrium gold nanoclusters quenched with biodegradable polymers. *ACS Nano 7*, 239−251.
(33) Simon, T., Boca, S. C., and Astilean, S. (2012) Pluronic-Nanogold hybrids: synthesis and tagging with photosensitizing molecules. *Colloids Surf., B: Biointerfaces 97*, 77−83.
(34) Tiwari, P., Vig, K., Dennis, V., and Singh, S. (2011) Functionalized gold nanoparticles and their biomedical applications. *Nanomaterials 1*, 31−63.
(35) Bogdanov, A. A., Weissleder, R., Frank, H. W., Bogdanova, A. V., Nossif, N., Schaffer, B. K., Tsai, E., Papisov, M. I., and Brady, T. J. (1993) A new macromolecule as a contrast agent for MR-angiography - preparation, properties, and animal studies. *Radiology 187*, 701−706.
(36) Bogdanov, A. J., Weissleder, R., and Brady, T. (1995) Long-circulating blood pool imaging agents. *Adv. Drug Delivery Rev. 16*, 335−348.
(37) Choi, Y. H., Liu, F., Kim, J. S., Choi, Y. K., Park, J. S., and Kim, S. W. (1998) Polyethylene glycol-grafted poly-L-lysine as polymeric gene carrier. *J. Controlled Release 54*, 39−48.
(38) Callahan, R. J., Bogdanov, A., Jr., Fischman, A. J., Brady, T. J., and Weissleder, R. (1998) Preclinical evaluation and phase I clinical trial of a 99mTc-labeled synthetic polymer used in blood pool imaging. *AJR Amer. J. Roentgenol. 171*, 137−143.
(39) Kleeff, J., Ishiwata, T., Kumbasar, A., Friess, H., Buchler, M. W., Lander, A. D., and Korc, M. (1998) The cell-surface heparan sulfate proteoglycan glypican-1 regulates growth factor action in pancreatic carcinoma cells and is overexpressed in human pancreatic cancer. *J. Clin. Invest. 102*, 1662−1673.
(40) Aikawa, T., Whipple, C. A., Lopez, M. E., Gunn, J., Young, A., Lander, A. D., and Korc, M. (2008) Glypican-1 modulates the angiogenic and metastatic potential of human and mouse cancer cells. *J. Clin. Invest. 118*, 89−99.
(41) Li, G., D'Souza-Schorey, C., Barbieri, M. A., Cooper, J. A., and Stahl, P. D. (1997) Uncoupling of membrane ruffling and pinocytosis during Ras signal transduction. *J. Biol. Chem. 272*, 10337−10340.
(42) Meng, H., Yang, S., Li, Z., Xia, T., Chen, J., Ji, Z., Zhang, H., Wang, X., Lin, S., Huang, C., Zhou, Z. H., Zink, J. I., and Nel, A. E. (2011) Aspect ratio determines the quantity of mesoporous silica nanoparticle uptake by a small GTPase-dependent macropinocytosis mechanism. *ACS Nano 5*, 4434−4447.
(43) Raoof, M., Cisneros, B. T., Corr, S. J., Palalon, F., Curley, S. A., and Koshkina, N. V. (2013) Tumor selective hyperthermia induced by short-wave capacitively-coupled RF electric-fields. *PLoS One 8*, e68506.
(44) Wang, Y., Liu, X., and Hnatowich, D. J. (2007) An improved synthesis of NHS-MAG3 for conjugation and radiolabeling of biomolecules with 99mTc at room temperature. *Nat. Protoc. 2*, 972−978.
(45) Rasmussen, S. R., Larsen, M. R., and Rasmussen, S. E. (1991) Covalent immobilization of DNA onto polystyrene microwells: the molecules are only bound at the 5′ end. *Anal. Biochem. 198*, 138−142.